ResGAT: Residual Graph Attention Network for Molecular Property Prediction

1st Thanh-Hoang Nguyen-Vo
School of Mathematics and Statistics
Victoria University of Wellington
Wellington, New Zealand
hoang.nguyen@weltec.ac.nz

2nd Binh P. Nguyen
School of Mathematics and Statistics
Victoria University of Wellington
Wellington, New Zealand
binh.p.nguyen@vuw.ac.nz

***Abstract*—Molecular property prediction is a crucial stage in the drug discovery pipeline. Many computational methods have been proposed to predict diverse types of molecular properties. Although recent approaches show promising outcomes, no single architecture can comprehensively address all tasks, making this area persistently challenging and demanding considerable time and effort. In addition to conventional machine learning and deep learning (DL) architectures that process regular data, several DL architectures designed for graph-structured data have been introduced to overcome the limitations of traditional methods. Utilizing graph-structured data in Quantitative Structure-Activity Relationship (QSAR) modeling presents an alternative that can enable models to effectively extract unique data features, particularly in scenarios where connectivity information is essential. In our study, we developed Residual Graph Attention Networks (ResGAT), a DL architecture that works with molecular graph-structured data. The proposed architecture is capable of addressing both regression and classification problems. Its practical design is customizable to adapt to various dataset sizes, improving the learning process based on molecular patterns. QSAR models developed using ResGAT demonstrated competitive performance compared to state-of-the-art methods under two data sampling strategies.**

***Index Terms*—graph attention network, graph convolutional network, residual, shortcut connection, molecular property prediction**

I. Introduction

Property prediction in the realm of modern drug discovery is an essential step, continuously capturing the utmost attention of researchers [1]. Accurate determination of molecular properties facilitates screening processes to identify potential drug candidates, contributing to an overall reduction in cost and time [2]. Since molecular structures and biological activities (or properties) are closely associated, many computational approaches have been developed to predict these properties based on structural information. Among these approaches, Quantitative Structure–Activity Relationship (QSAR) modeling is a cost-effective computational method frequently used to predict diverse molecular properties (e.g., lipophilicity, hydrophobicity, solubility) [3]. These QSAR models are flexibly designed and optimized for efficient learning of intricate structural patterns. Despite initial successes, these modeling tasks continue to pose significant challenges due to the complexity of chemical structures, class imbalance, high-dimensional data representation, and low data volume. To partially address these challenges, developing robust computational methods and promoting interdisciplinary collaboration are highly required.

In the past two decades, there has been a notable emergence of the Graph Neural Network (GNN) [4], specifically developed to handle molecular graphs [5]–[9]. The development of efficient GNN variants enables the advent of graph-based representation learning [10]–[13]. For years, numerous studies have employed GNN and its variants for molecular property prediction. Scarselli *et al.* [4] proposed the first version of GNN in 2009. Although GNN can handle graph-structured data, their applications have not been widespread due to their relatively low learning efficiency until the Graph Convolutional Network (GCN) was presented [14]. The introduction of GNN has sparked a significant amount of further research and extensive practice in graph-based deep learning (DL) architectures. In 2020, Wieder *et al.* [15] conducted a critical review to summarize DL architectures used for molecular property prediction. Gilmer *et al.* [16] developed neural fingerprints using CNN customized for graph-structured data. After critically surveying various GNN-based models, Yang *et al.* [17] introduced and conceptualized the Message Passing Neural Network (MPNN), characterized by two distinct phases: *Message Passing* and *Readout*. Yang *et al.* [18] presented directed MPNN (D-MPNN) as an upgraded version of MPNN that prioritizes updating information specifically on directed bonds instead of atoms. Xiong *et al.* [10] introduced AttentiveFP, an attention-based network that achieved robust performance on multiple benchmark datasets. The HRGCN+, by Wu *et al.* [11], combines molecular graphs and descriptors (physicochemical features) to boost prediction efficiency with excellent performance compared to existing methods. Li *et al.* [8] proposed the Triplet Message Network (TrimNet) for processing molecular graphs, an architecture designed to significantly reduce the number of parameters and enhance the capacity to extract bonding information. The Graph Multiset Transformer (GMT), developed by Baek *et al.* [19], is a Transformer-based architecture adapting to multiset pooling

The work was supported in part by the Faculty Strategic Research Grant (FSRG) number 411494 at Victoria University of Wellington (VUW) and the Endeavour Fund (Smart Ideas) from the New Zealand Ministry of Business, Innovation and Employment (MBIE) under contract VUW RTVU2301.

on graphs. Most recently, the Hierarchical Informative Graph Neural Network (HiGNN), by Zhu *et al*. [9], is one of the most competitive DL architectures. HiGNN comprises two main blocks: *Atom-Atom Interaction* and *Feature-Wise Attention*. The Atom-Atom Interaction block is based on neural tensor networks for knowledge graph reasoning [20], while the Feature-Wise Attention block recalibrates an atom's representations after the Message Passing phase, thus enhancing the selective extraction of important features. Initially, the model's input, the molecular structure, is fragmented into substructures using the BRICS algorithm [21], creating global and hierarchical molecular representations. Since the implementation of HiGNN requires high computational costs to process graph-structured data, it may not be cost- or time-effective for prediction tasks on large datasets. Moreover, the effectiveness of using complex attention mechanisms might not always align with expectations. The performance of models is influenced by various factors, including the complexity of the tasks, data quality, and volume. In such scenarios, architectures with simpler attention mechanisms could offer a more appropriate alternative.

Although many models have been introduced for molecular property prediction, there is still a large room for further improvement. The prediction efficiency heavily depends on the availability of high-quality data, the chemical diversity of datasets, and data curation processes. Insufficient or biased data can limit the model's ability to learn molecular patterns and predict accurately. Besides, computational cost is also an essential issue that needs to be managed when dealing with extensive sets of molecules. Computationally expensive methods may make them impractical for upscaling models. On the other hand, generalizability is one of the problems found in most computational methods. Models developed or evaluated on specific sets of molecules for certain properties may not inefficiently perform on other datasets or completely new data, especially when the training data are not good representatives. In spite of being tested against multiple benchmark datasets, all known state-of-the-art methods remain susceptible to failure when applied to a new prediction task. Developing novel methods for molecular property prediction, therefore, is always one of the key topics in modern drug discovery to address various prediction tasks in the future.

In this study, we present the Residual Graph Attention Network (ResGAT), a novel graph-based DL architecture for molecular property prediction tasks. This architecture is constructed from two key insights: the utilization of *(1) regular shortcut connections between blocks* and *(2) shortcut connections impeded by a graph attention layer*. The introduction of these two types of shortcut connections into the ResGAT helps enhance model learning capacity by stabilizing the training process and generalization. Our architecture can be applied to address both regression and classification problems. Importantly, the number of blocks per block set can be flexibly customized to adapt to various dataset sizes. ResGAT was benchmarked against two baselines and five state-of-the-art architectures on nine benchmark molecular datasets.

II. Proposed Architecture

A. Residual Graph Attention Network

We introduce the Residual Graph Attention Network (ResGAT), as described in Algorithm 1, a unique DL architecture designed to process graph-structured data and capable of addressing a variety of molecular property prediction tasks. The ResGAT architecture is constructed using *Graph Attention (GAT)* layers [22] and two types of *shortcut connections* [23]. GAT, a masked self-attention layer, is demonstrated to outperform the GCN layer in terms of computing speed and efficiency (see *Subsection II-B*). The *shortcut connection* is a crucial component of Residual Neural Networks (ResNet) [23]. This architecture is designed with three *Block Sets*, and each of them is specified by L blocks (Figure 1). A single block consists of two GAT layers activated by the rectified linear unit (ReLU) function. After passing *Block Set 3*, the outputs are pooled with a Global Max-pooling layer. Finally, the max-pooled outputs are passed through a Fully Connected (FC) block comprising three layers. The first two layers are activated by the ReLU function, while the final layer is activated by the Sigmoid function for classification tasks or by the ReLU function for regression tasks. In comparison with ResNet, ResGAT architectures have a smaller number of layers in each block. In ResNet, each block comprises a minimum of four CNN layers, whereas in ResGAT, each block consists of just two GAT layers. Furthermore, we employed another shortcut connection impeded by a graph attention layer, referred to as the '*graph attention shortcut*'. This concept is inspired by a critical analysis conducted by He *et al*. [23] about the propagation formulations used in residual building blocks with diverse types of shortcut connections. Integrating these two types of shortcut connections into the ResGAT enhances the model's learning capacity by stabilizing the training process and improving generalization. In addition to the main architecture, ResGAT, we also developed a generic version named ResGCN, which differs only in that all GAT layers [22] are replaced with GCN layers [14].

Algorithm 1 ResGAT

procedure ResGAT (or ResGCN)(x)
  Initialize graph attention layer: GAT (or GCN)
  Initialize basic blocks: basic_block
  $x \leftarrow$ ReLU (GAT(x)) ▷ graph attention layer 1
  $x \leftarrow$ ReLU (GAT(x)) ▷ graph attention layer 2
  Initialize global max pooling: GMP
  Initialize fully connected layer: FC
  $x \leftarrow$ GAT(x) ▷ Input graph attention layers
  for $k = 1$ to 3 **do** ▷ No. of block sets
    for $l = 1$ to L **do** ▷ No. of blocks in block set k
      if $l = 1$ **then**
        $x \leftarrow x$ + GAT(x)
      else if **then**
        $x \leftarrow x$ + basic_block^l
      end if
    end for
  end for
  $x \leftarrow$ GMP(x) ▷ Global max pooling
  $x \leftarrow$ FC(x) ▷ Fully connected layer
  return x
end procedure

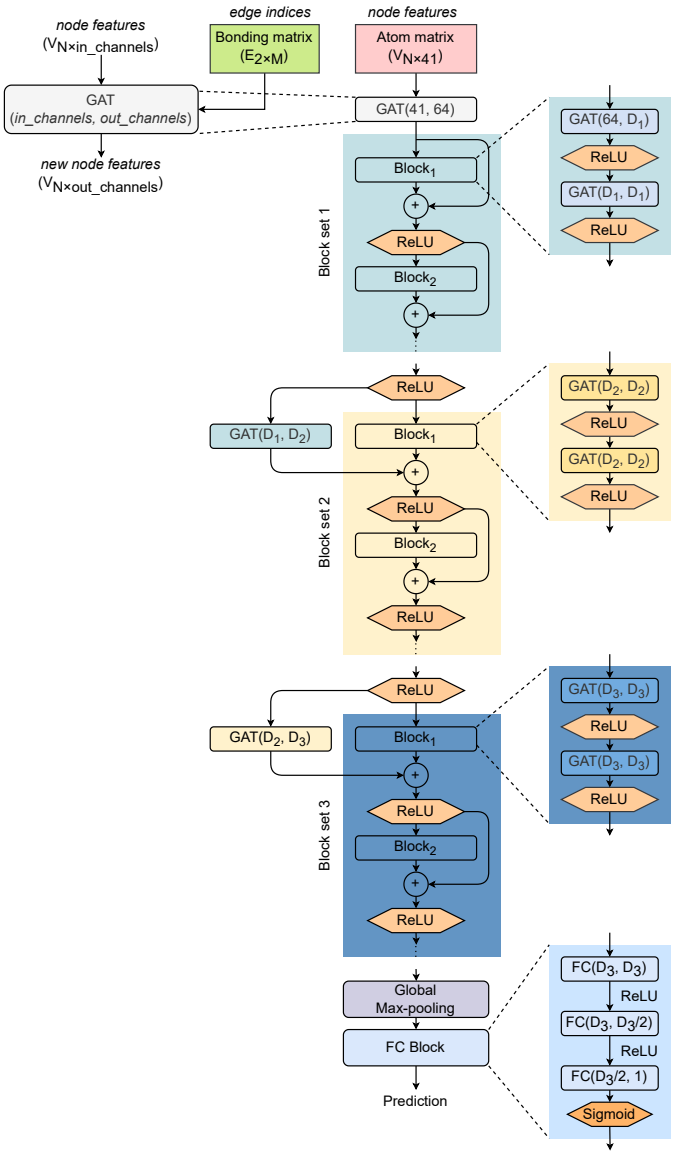

Fig. 1. Architecture of ResGAT.

B. Graph Attention Layer

The Graph Attention (GAT) layer was completely formulated by Veličković *et al*. [22] based on a previously published work done by Bahdanau *et al*. [24]. A graph $\mathcal{G}(\mathcal{V}, \mathcal{E})$ with N nodes (vertices) is defined by a vector of node features $h = \{ h_1, h_2, h_3, ..., h_N\}$ with $h \in \mathbb{R}^F$. The vector h is operated by the GAT layer to return $h' = \{h'_1, h'_2, h'_3, ..., h'_N\}$ with $h' \in \mathbb{R}^{F'}$. The weight matrix $\mathbf{W} \in \mathbb{R}^{F' \times F}$ is multiplied to every node; and F and F' are the numbers of input and output features, respectively. The attention output e_{uv} of node$_u$ directed from node$_v$ is computed as:

$$e_{uv} = a(\mathbf{W}h_u, \mathbf{W}h_v) = ReLU(a^T \odot [\mathbf{W}h_u || \mathbf{W}h_v]), \quad (1)$$

where a is the self-attention feedforward layer parameterized by the learnable vector of parameters a^T and $||$ denotes the concatenation operation. The Softmax function is applied to normalize the attention output. Each normalized attention output α_{uv} is computed as:

$$\alpha_{uv} = Softmax(e_{uv}) = \frac{\exp(e_{uv})}{\sum_{k \in \mathcal{N}(u)} \exp(e_{uk})}. \quad (2)$$

The equation for α_{uv} is rewritten as:

$$\alpha_{uv} = \frac{\exp(ReLU(a^T \odot [\mathbf{W}h_u || \mathbf{W}h_v])}{\sum_{k \in \mathcal{N}(u)} \exp(ReLU(a^T \odot [\mathbf{W}h_u || \mathbf{W}h_k])}. \quad (3)$$

Since the layer is designed to force each node to attend to all other nodes in the network, the output vector of node$_u$ ($\vec{h'}_u$) is finally obtained by the summation of all products of the normalized attention outputs (α_{uv}) and the weighted node feature vectors (h_v) of other neighboring nodes.

$$h'_u = \sigma(\sum_{v \in \mathcal{N}(u)} \alpha_{uv} \odot \mathbf{W}h_v), \quad (4)$$

where σ is the nonlinearity activation function.

III. Experiments

A. Overview

The major steps in our experiments are presented in Figure 2. First, the original benchmark datasets were downloaded from MoleculeNet [25]. To qualify the data for the modeling experiment, all the benchmark datasets were curated (see *Subsection III-C*) before being encoded (see *Subsection III-D*). Then, each refined dataset was divided into two parts: a train-val set and a test set with a ratio of 90:10. The train-val data was then split into a new training set and a validation set with a ratio of 90:10. The validation set was used for hyperparameter tuning. Once hyperparameter tuning was completed, the model was retrained using the best hyperparameters, and then it was evaluated using the test set for benchmarking (see *Subsection III-F*).

B. Benchmark Datasets

To investigate the performance of ResGAT, we conducted a large number of modeling experiments on nine benchmark molecular datasets, including ESOL, FreeSolv, Lipo, BACE, BBBP, HIV, ClinTox, SIDER, and Tox21. These datasets were collected from MoleculeNet [25], an online source of molecular datasets specially designed to benchmark machine learning methods on property prediction tasks. Table I gives information on the datasets used in the study. After collecting these datasets, we performed data curation to remove unqualified samples. Generally, the number of samples from all refined datasets decreased after the data curation was completed (Table II). The details of data curation are provided in *Subsection III-C*.

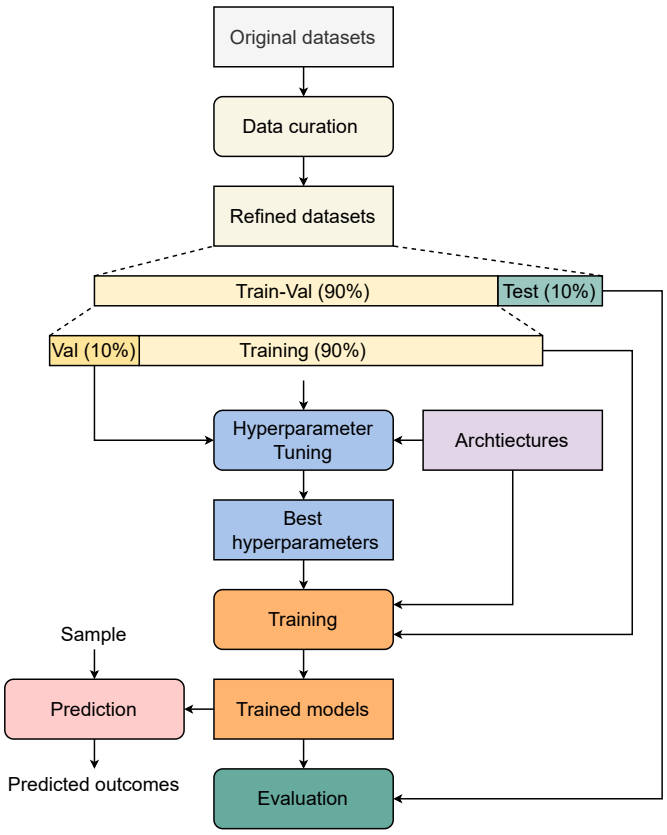

Fig. 2. Flowchart of our experiments.

TABLE I
LIST OF BENCHMARK DATASETS

Task type	Dataset	# tasks	Evaluation metric
Regression	ESOL	1	RMSE
	FreeSolv	1	RMSE
	Lipo	1	RMSE
Classification	BACE	1	AUCROC
	BBBP	1	AUCROC
	HIV	1	AUCROC
	ClinTox	2	AUCROC
	SIDER	27	AUCROC
	Tox21	12	AUCROC

C. Data Curation

Before conducting experiments, we performed data curation to qualify the chemical data for model development and evaluation. Our curation pipeline was implemented based on Fourches *et al.* [26]'s criteria for chemical data used in QSAR modeling, with minor modifications. This pipeline is designed with four phases: *(1) Validation*, *(2) Cleaning*, *(3) Normalization*, and *(4) Final verification*. Before entering the pipeline, all chemical data (in SMILES format) were converted into their corresponding canonical forms. In phase *(1)*, molecules whose chemical types belong to one of three classes, including inorganics, mixtures, and organometallics, are removed. In phase *(2)*, salts and manipulating charged molecules are eliminated. Charged molecules may be formed by metal-containing structures or polar organic groups. While metal-containing charged molecules are rejected, organic charged molecules are converted to non-charged forms. The neutralization of charged organic molecules, however, remains a controversial topic among scientists, as they face challenges in precisely determining the experimental conditions under which these molecules exhibit activities. In phase *(3)*, detautomerization, destereoisomerization, and removal of chemotypes are executed to unify tautomers, stereoisomers, or chemotypes of the same molecules into canonical forms. A molecule possessing unstable substructures often undergoes interchange among multiple intermediate forms. When considering a group of tautomers (or chemotypes) for the same molecule, the intermediate form that exhibits the highest degree of structural equivalence compared to other forms is selected as the canonical tautomer (or chemotype). At the end of these three first phases, any duplicates found are discarded. In phase *(4)*, samples (molecules) whose labels conflict with each other are manually processed. Conflicting samples can arise in any of the three situations outlined below: (a) a group of identical molecules with different labels; (b) a group of identical molecules with duplicated labels; and (c) a group of different molecules identified by the same CAS registry number. Samples in situations (a) or (c) are excluded, whereas those in situations (b) are retained and unified. Finally, structural verification is accomplished to confirm identity and validity using the two largest chemical databases: PubChem and ChEMBL. Table II compares the number of samples in refined datasets with the original ones.

TABLE II
NUMBER OF SAMPLES IN EACH BENCHMARK DATASET AFTER CURATION

Task type	Dataset	# samples	
		Original	Refined
Regression	ESOL	1128	1115
	FreeSolv	642	635
	Lipo	4200	4100
Classification	BACE	1513	1454
	BBBP	2050	1760
	HIV	41127	38094
	ClinTox	1484	1349
	SIDER	1427	1225
	Tox21	7831	7381

D. Molecular Encoding Scheme

Figure 3 explains the molecular encoding scheme used in our study. For each molecule constituted by N heavy atoms (excluding hydrogen) and M bonds connecting these atoms, its representations are defined with two matrices: an atom matrix with a dimension of $N \times 41$ and a bonding matrix with a dimension of $M \times 2$. The values of N and M vary across molecules.

The atom matrix is created in several steps. The molecular structure is first analyzed to determine the appearance order of heavy atoms, and these atoms are then assigned indices. For each atom, a set of 41 features is computed using the RDKit library [27]. The details of these features are described

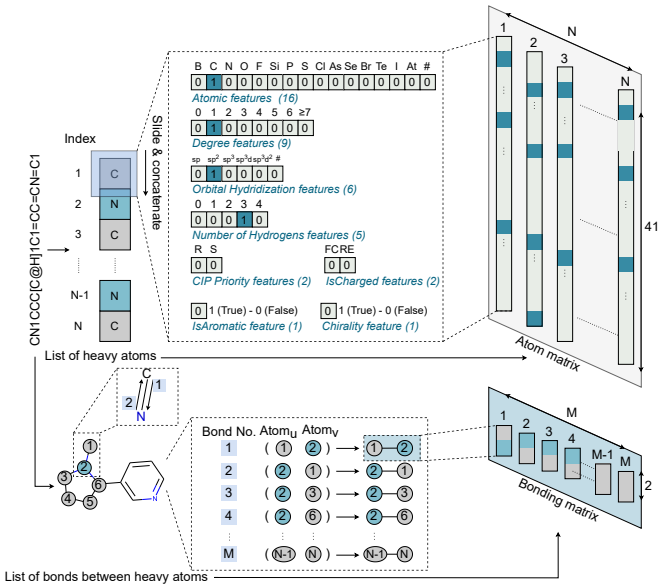

Fig. 3. Molecular encoding scheme.

in Table III. For a heavy atom, a 41-dimensional feature vector is organized as a binary vector with a size of 1×41. The feature vector consists of 16 *Atomic* features, 9 *Degree* features, 6 *Orbital Hybridization* features, 5 *Number of Hydrogens* features, 2 *Cahn-Ingold-Prelog (CIP) Priority* features, 2 *IsCharge* features, 1 *IsAromatic* feature, and 1 *Chirality* feature. The *Atomic* features determine the atom based on the atom list. The *Degree* features indicate the number of bonds formed by the atom with neighboring heavy atoms, ranging from 0 to 8. The *Orbital Hybridization* features describe the specific type of orbital hybridization of a heavy atom uses to form its bonds. The *Number of Hydrogens* feature counts the number of hydrogen atoms that have bonds with a heavy atom. The *CIP Priority* features identify the spatial orientation of a chiral center (atom bonding to four different groups): clockwise (R) or counterclockwise (S). The *IsCharge* features present the charge state of an atom to assign it either the '*Formal Charge (FC)*' or '*Radical Electron (RE)*' state. The *IsAromatic* feature defines whether an atom is a member of any ring or cyclic structure. The *Chirality* feature identifies whether a heavy atom has a chiral center. To create the bond matrix, the connectivity map of all heavy atoms is computed (as shown in Figure 3). The atom matrix carries information on the node features, while the bond matrix stores information on the edge indices.

E. Model Development

While GAT is flexible in learning graph structures with highly varying neighbor relationships, it requires a higher number of parameters to learn attention coefficients. In contrast, GCN is parameter-efficient due to shared weights across the graph but may struggle with generalizability when faced with new graph patterns. GCN is well-suited for relatively uniform or well-defined graph patterns, while GAT is more

TABLE III
FEATURE ENCODING OF A HEAVY ATOM

Feature type	# features	Details
Atomic	16	B, C, N, O, F, Si, P, S, Cl, As, Se, Br, Te, I, At, others
Degree	8	0, 1, 2, 3, 4, 5, 6, 7
Orbital Hybridization	6	sp, sp^2, sp^3, sp^3d, sp^3d^2, others
Number of Hydrogens	5	0 ,1, 2, 3, 4
CIP Priority	2	R (Clockwise), S (Counter-clockwise)
IsCharge	2	Formal Charge, Radical Electron
IsAromatic	1	Aromaticity, Non-aromaticity
Chirality	1	Chiral center, Not chiral center
Total	41	A feature vector of a heavy atom

appropriate for handling complex graph structures. To address diverse scenarios, we introduce another variant of the ResGAT architecture named ResGCN, wherein all GAT layers are replaced with GCN layers.

All models constructed with these two architectures were tuned, trained, and tested under the same conditions and settings. For each dataset, the training and validation sets were used for model tuning and development, while the test set was used for model evaluation. Test sets were not involved in any stage of model selection. Initially, the number of blocks (`num_block`) in each block set was fixed at 1 to tune the feature embedding size (`embed_size`) of the graph layer with three values of 64, 128, and 256. After tuning the parameter `embed_size` for a block in each block set, we tuned the parameter `num_block` for each block set with three values of 1, 2, and 3. Finally, the learning rate was tuned with three values of 1×10^{-4}, 5×10^{-4}, and 1×10^{-3}. Models implemented for different prediction tasks have different hyperparameters. The loss functions for regression and classification tasks are Mean Squared Error (MSE) and Binary Cross Entropy (BCE), respectively, and are computed as:

$$Loss_{MSE} = \frac{1}{n}\sum_{i=1}^{n}(y_i - \hat{y}_i)^2, \tag{5}$$

$$Loss_{BCE} = \frac{1}{n}\sum_{i=1}^{n} y_i \cdot \log(\hat{y}_i) + (1 - y_i) \cdot \log(1 - \hat{y}_i), \tag{6}$$

where n is the number of samples; y is the ground truth (label), and $\hat{y}$ is the predicted value or probability of the regression or classification task, respectively.

F. Model Evaluation

To examine the efficiency of ResGAT, we developed a series of prediction models using ResGAT and other state-of-the-art architectures, including AttentiveFP [10], GMT [19], TrimNet [8], D-MPNN [18], and HiGNN [9]. The GCN [14] and GAT [22] architectures were also used to develop two baseline graph models. Models of state-of-the-art architectures were reimplemented using source codes provided by their authors. The parameters of all reimplemented models were also fairly tuned. Besides, two sampling methods, *random* and *scaffold*, were employed. For each dataset, the modeling

experiment for a particular architecture was repeated ten times to avoid sampling bias.

To evaluate all models, we used the Root Mean Squared Error (RMSE) and the Area Under the Receiver Operating Characteristic (ROC) curve (AUCROC) for regression tasks and classification tasks, respectively. For multitask classification tasks, the average AUCROC was computed based on the number of tasks. Our code is made publicly available in our GitHub repository[1].

IV. Experimental Results and Discussion

A. Results

Experimental results show that ResGAT and ResGCN have equivalent performance in all classification tasks under both sampling strategies (Figure 4). Under the random sampling strategy, ResGCN has slightly lower performance on the BACE, BBBP, and HIV datasets but higher performance on the ClinTox dataset compared to ResGAT. The performances of both models on the SIDER and Tox21 datasets are almost similar. For the regression tasks, ResGCN obtains higher performance on all datasets compared to ResGAT. Under the scaffold sampling strategy, ResGCN shows greater efficiency on the ESOL dataset, whereas ResGAT obtains better performance on the FreeSolve dataset. Their effectiveness on the Lipo dataset is comparable. For classification tasks, ResGCN achieves higher performance on the BBBP and ClinTox datasets. Meanwhile, ResGAT works effectively on the BACE dataset only. Both models demonstrate similar levels of prediction power on the rest of the classification datasets.

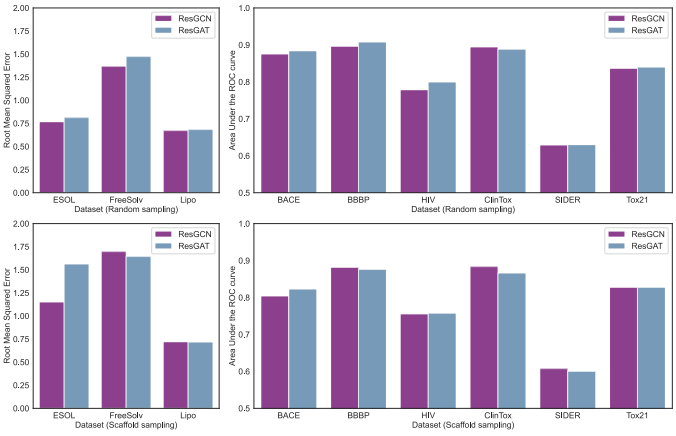

Fig. 4. Performance of ResGAT and ResGCN under two sampling strategies.

Tables IV, V, and VI provide detailed results of modeling experiments on nine benchmark datasets of regression, binary classification, and multitask classification tasks, respectively. These tables compare the performance of the models constructed using our proposed architecture with those constructed using state-of-the-art architectures. The experimental results show that our models (developed using ResGAT or ResGCN) are ranked in the top 3 in five out of the nine datasets and in seven out of the nine datasets under the random sampling and scaffold sampling strategies, respectively. Under the random sampling strategy, our models obtain three 1^{st}-ranks on the BACE, HIV, and ClinTox datasets; two 2^{nd}-ranks on the ClinTox and SIDER datasets; and three 3^{rd}-ranks on the FreeSolve, BACE, and SIDER datasets. Under the scaffold sampling strategy, our models achieve two 2^{nd}-ranks (on the FreeSolv and BACE datasets) and three 3^{rd}-ranks (on the Lipo, BBBP, and HIV datasets). D-MPNN is a very robust architecture when 13 D-MPNN-based models are ranked in the top-3 of both sampling strategies. However, most of them obtain only 2^{nd}-ranks and 3^{rd}-ranks. Also, HiGNN is an efficient architecture compared to others. Although there are only nine out of eighteen HiGNN-based models present in the top 3, they had seven 1^{st}-ranks on the ESOL, Lipo, BACE, BBBP, HIV, and ClinTox datasets. The TrimNet and GMT architectures work better on regression tasks while showing low predictive efficiency in classification tasks. Models implemented using the AttentiveFP architecture achieve competitive performance on classification tasks, especially for those with a large number of tasks. To rank the overall performance of all implemented architectures, we create a summary table describing the performance ranking of the models on the test sets. For each dataset, the performance of models is ranked from 1 (highest) to 9 (smallest) scores. Every architecture is assigned scores from nine datasets. The maximum score is 81, and the minimum score is 9 (Table VII). Based on average ranking scores, the ResGAT and ResGCN are in the top 3. Under the random sampling strategy, D-MPNN and HiGNN have the smallest average ranking scores of 3.22, followed by ResGAT (3.33), ResGCN (3.89), and others. Under the scaffold sampling strategy, D-MPNN achieves average ranking scores of 3.22, followed by ResGAT (3.44), ResGCN (3.89), and others.

TABLE IV
Performance of Different Regression Models

Sampling	Model	Dataset		
		ESOL	FreeSolv	Lipo
Random	GCN	2.0569±0.14	3.6618±0.75	1.1974±0.03
	GAT	2.4261±0.16	4.4315±0.87	1.4974±0.06
	AttentiveFP	1.5225±0.13	3.5585±0.72	1.1232±0.03
	GMT	0.7072±0.08	1.3568±0.16	0.7068±0.03
	TrimNet	0.7499±0.04	1.5996±0.16	0.6315±0.03
	D-MPNN	0.6930±0.08	**1.1394±0.18**	0.6148±0.03
	HiGNN	**0.6029±0.07**	1.8917±0.32	**0.6033±0.01**
	ResGCN	0.7683±0.09	1.3687±0.20	0.6721±0.02
	ResGAT	0.8125±0.07	1.4734±0.31	0.6833±0.02
Scaffold	GCN	3.0413±0.02	1.9055±0.11	1.1347±0.04
	GAT	3.6433±0.11	2.7487±0.40	1.3925±0.06
	AttentiveFP	2.5073±0.11	2.9627±0.23	1.1516±0.09
	GMT	**0.9009±0.05**	1.6893±0.12	0.7467±0.04
	TrimNet	1.1321±0.08	**1.5290±0.27**	**0.6514±0.03**
	D-MPNN	1.0731±0.01	1.6688±0.01	0.6525±0.07
	HiGNN	5.2009±0.01	4.8752±0.01	1.6644±0.01
	ResGCN	1.1509±0.09	1.6966±0.12	0.7208±0.05
	ResGAT	1.5622±0.12	1.6430±0.22	0.7173±0.04

In our experiments, we implemented all DL models using PyTorch 1.12.0 and PyTorch Geometric 2.0.4, training them

[1]The Github link was removed for double-blind review, and it will be made publicly available upon acceptance of the paper.

TABLE V
PERFORMANCE OF DIFFERENT CLASSIFICATION MODELS

Sampling	Model	Dataset		
		BACE	BBBP	HIV
Random	GCN	0.6505±0.03	0.6155±0.06	0.6245±0.04
	GAT	0.6316±0.06	0.6338±0.07	0.5310±0.05
	AttentiveFP	0.8836±0.04	0.9129±0.04	0.7878±0.01
	GMT	0.7859±0.04	0.8752±0.05	0.4106±0.02
	TrimNet	0.8054±0.05	0.8275±0.03	0.7333±0.02
	D-MPNN	0.8788±0.04	**0.9197±0.03**	0.5134±0.09
	HiGNN	0.8656±0.04	0.9249±0.03	0.7891±0.02
	ResGCN	0.8752±0.03	0.8959±0.05	0.7786±0.01
	ResGAT	**0.8840±0.03**	0.9077±0.02	**0.7995±0.01**
Scaffold	GCN	0.6150±0.05	0.5914±0.06	0.6143±0.05
	GAT	0.6053±0.11	0.6331±0.05	0.5626±0.04
	AttentiveFP	0.8108±0.05	0.8816±0.04	0.7800±0.04
	GMT	0.7739±0.05	0.8519±0.06	0.4153±0.06
	TrimNet	0.7071±0.05	0.8694±0.03	0.7563±0.03
	D-MPNN	0.8191±0.02	0.8784±0.04	0.4425±0.03
	HiGNN	**0.8312±0.01**	**0.9121±0.01**	**0.7813±0.02**
	ResGCN	0.8040±0.03	0.8813±0.03	0.7555±0.04
	ResGAT	0.8227±0.03	0.8757±0.04	0.7573±0.06

TABLE VI
PERFORMANCE OF DIFFERENT MULTITASK CLASSIFICATION MODELS

Sampling	Model	Dataset		
		ClinTox	SIDER	Tox21
Random	GCN	0.4668±0.03	0.5392±0.04	0.6078±0.04
	GAT	0.5329±0.07	0.5618±0.05	0.4828±0.04
	AttentiveFP	0.8459±0.02	**0.6409±0.06**	**0.8600±0.05**
	GMT	0.8701±0.01	0.5825±0.10	0.5000±0.01
	TrimNet	0.6970±0.06	0.5456±0.07	0.8451±0.04
	D-MPNN	0.8531±0.01	0.5921±0.05	0.8479±0.05
	HiGNN	0.8503±0.02	0.6165±0.05	0.8431±0.05
	ResGCN	**0.8944±0.01**	0.6290±0.05	0.8361±0.05
	ResGAT	0.8881±0.01	0.6300±0.05	0.8397±0.05
Scaffold	GCN	0.5123±0.08	0.5106±0.04	0.5911±0.04
	GAT	0.5473±0.02	0.5328±0.05	0.4760±0.07
	AttentiveFP	0.8505±0.01	0.5710±0.06	0.8492±0.05
	GMT	0.8505±0.01	0.5443±0.04	0.5000±0.01
	TrimNet	0.7076±0.05	0.5995±0.08	0.8140±0.06
	D-MPNN	0.8726±0.05	**0.6095±0.07**	**0.8455±0.05**
	HiGNN	**0.9212±0.04**	0.5892±0.05	0.8446±0.05
	ResGCN	0.8835±0.03	0.6075±0.06	0.8272±0.06
	ResGAT	0.8661±0.01	0.6000±0.06	0.8273±0.06

on an i9-13900K with 64 GB of RAM and one NVIDIA GTX 3060. The training process time (seconds per epoch), recorded in Table VIII, reflects the computing resources required. Our models demonstrate superior time and cost efficiency compared to state-of-the-art models, notably outperforming D-MPNN- and HiGNN-based models with up to a 50% reduction in training time. While only models developed with two baseline architectures (GCN and GAT) have shorter training times, for the ClinTox dataset, ResGCN-based models exhibit slightly higher training times than other models, whereas ResGAT-based models still require less time. Testing completion for our models ranged from 0.02 to 0.48 seconds, depending on the dataset, comparable to the two baseline models and faster than all other models. In summary, the results confirm that our proposed architectures are not only robust but also time-effective.

B. Discussion

Besides achieving goals, our proposed architecture still has limitations that need to be improved in the future. Overall, compared to D-MPNN and HiGNN, ResGAT (and ResGCN) show less efficiency in regression problems. In binary classification tasks, ResGAT obtains better performance under the random sampling strategy, while HiGNN demonstrates its powerful architecture under the scaffold sampling strategy. In multitask classification tasks, although ResGAT works more effectively than HiGNN under the random sampling strategy, its performance under the scaffold sampling strategy needs to be enhanced. From our experimental results, it can be observed that our proposed architecture is more efficient when dealing with classification tasks than regression tasks. It can work competently on large datasets, especially for multitask classification problems.

V. CONCLUSIONS

In this study, we presented ResGAT, an innovative DL architecture designed for predicting molecular properties from graph-structured data. ResGAT is versatile, capable of handling both regression and classification tasks, and it offers a flexible tuning mechanism to accommodate various dataset sizes. The depth of the architecture can be adjusted to specific needs, and our experimental findings validate its robustness and efficiency. Our results highlight that ResGAT, along with ResGCN, are compelling architectures warranting further exploration to enhance predictive capabilities.

REFERENCES

[1] Y. Tang, W. Zhu, K. Chen, and H. Jiang, "New technologies in computer-aided drug design: Toward target identification and new chemical entity discovery," *Drug Discovery Today: Technologies*, vol. 3, no. 3, pp. 307–313, 2006.

[2] J. Shen and C. A. Nicolaou, "Molecular property prediction: recent trends in the era of artificial intelligence," *Drug Discovery Today: Technologies*, vol. 32-33, pp. 29–36, 2019.

[3] V. Bastikar, A. Bastikar, and P. Gupta, "Quantitative structure–activity relationship-based computational approaches," in *Computational Approaches for Novel Therapeutic and Diagnostic Designing to Mitigate SARS-CoV-2 Infection*. Elsevier, 2022, pp. 191–205.

[4] F. Scarselli, M. Gori, A. C. Tsoi, M. Hagenbuchner, and G. Monfardini, "The graph neural network model," *IEEE Transactions on Neural Networks*, vol. 20, no. 1, pp. 61–80, 2009.

[5] I. I. Baskin, V. A. Palyulin, and N. S. Zefirov, "A neural device for searching direct correlations between structures and properties of chemical compounds," *Journal of Chemical Information and Computer Sciences*, vol. 37, no. 4, pp. 715–721, 1997.

[6] A. Micheli, A. Sperduti, A. Starita, and A. M. Bianucci, "Analysis of the internal representations developed by neural networks for structures applied to quantitative structure-activity relationship studies of benzodiazepines," *Journal of Chemical Information and Computer Sciences*, vol. 41, no. 1, pp. 202–218, 2000.

[7] A. Goulon, T. Picot, A. Duprat, and G. Dreyfus, "Predicting activities without computing descriptors: graph machines for QSAR," *SAR and QSAR in Environmental Research*, vol. 18, no. 1-2, pp. 141–153, 2007.

[8] P. Li, Y. Li, C.-Y. Hsieh, S. Zhang, X. Liu, H. Liu, S. Song, and X. Yao, "TrimNet: learning molecular representation from triplet messages for biomedicine," *Briefings in Bioinformatics*, vol. 22, no. 4, 2020.

[9] W. Zhu, Y. Zhang, D. Zhao, J. Xu, and L. Wang, "HiGNN: A hierarchical informative graph neural network for molecular property prediction equipped with feature-wise attention," *Journal of Chemical Information and Modeling*, vol. 63, no. 1, pp. 43–55, 2022.

TABLE VII
PERFORMANCE RANKING OF DIFFERENT MODELS ON DIFFERENT DATASETS

Sampling	Model	Dataset									Average rank
		ESOL	FreeSolv	Lipo	BACE	BBBP	HIV	ClinTox	SIDER	Tox21	
Random	GCN	8	8	8	8	9	6	9	9	7	8.00
	GAT	9	9	9	9	8	7	8	7	9	8.33
	AttentiveFP	7	7	7	2	3	3	6	**1**	**1**	4.11
	GMT	3	2	6	7	6	9	3	6	8	5.56
	TrimNet	4	5	3	6	7	5	7	8	3	5.33
	D-MPNN	2	**1**	2	3	2	8	4	5	2	**3.22**
	HiGNN	**1**	6	**1**	5	**1**	2	5	4	4	**3.22**
	ResGCN	5	3	4	4	5	4	**1**	3	6	3.89
	ResGAT	6	4	5	**1**	4	**1**	2	2	5	3.33
Scaffold	GCN	7	6	6	8	9	6	9	9	7	7.44
	GAT	8	7	8	9	8	7	8	8	9	8.00
	AttentiveFP	6	8	7	4	2	2	5	6	**1**	4.56
	GMT	**1**	4	5	6	7	9	5	7	8	5.78
	TrimNet	3	**1**	**1**	7	6	4	7	4	6	4.33
	D-MPNN	2	3	2	3	4	8	3	**1**	2	**3.22**
	HiGNN	9	9	9	**1**	**1**	**1**	**1**	5	3	4.33
	ResGCN	4	5	4	5	3	5	2	2	5	3.89
	ResGAT	5	2	3	2	5	3	4	3	4	3.44

TABLE VIII
TRAINING TIME IN SECONDS FOR DIFFERENT MODELS USING DIFFERENT TRAINING DATASETS

Model	Dataset								
	ESOL	FreeSolv	Lipo	BACE	BBBP	HIV	ClinTox	SIDER	Tox21
GCN	**0.08**	0.07	0.48	0.13	0.16	4.12	**0.07**	**0.16**	**0.32**
GAT	0.10	**0.06**	**0.47**	**0.12**	**0.12**	**3.89**	**0.07**	0.17	0.48
AttentiveFP	0.39	0.17	1.01	0.50	0.47	10.06	0.10	0.42	0.69
GMT	0.57	0.24	0.82	0.63	0.68	6.51	0.40	0.62	1.02
TrimNet	0.84	0.27	0.98	0.83	0.63	6.57	0.44	0.85	1.51
D-MPNN	1.18	0.41	1.17	0.43	0.69	12.73	0.36	1.29	0.51
HiGNN	1.99	0.60	1.40	0.54	0.64	6.93	0.47	1.75	0.48
ResGCN	0.42	0.19	0.51	0.21	0.31	6.21	0.53	0.45	0.53
ResGAT	0.37	0.17	**0.47**	0.31	0.43	5.13	0.35	0.32	0.63

[10] Z. Xiong, D. Wang, X. Liu, F. Zhong, X. Wan, X. Li, Z. Li, X. Luo, K. Chen, H. Jiang, and M. Zheng, "Pushing the boundaries of molecular representation for drug discovery with the graph attention mechanism," *Journal of Medicinal Chemistry*, vol. 63, no. 16, pp. 8749–8760, 2019.

[11] Z. Wu, D. Jiang, C.-Y. Hsieh, G. Chen, B. Liao, D. Cao, and T. Hou, "Hyperbolic relational graph convolution networks plus: a simple but highly efficient QSAR-modeling method," *Briefings in Bioinformatics*, vol. 22, no. 5, 2021.

[12] P. Li, J. Wang, Y. Qiao, H. Chen, Y. Yu, X. Yao, P. Gao, G. Xie, and S. Song, "An effective self-supervised framework for learning expressive molecular global representations to drug discovery," *Briefings in Bioinformatics*, vol. 22, no. 6, 2021.

[13] H. Cai, H. Zhang, D. Zhao, J. Wu, and L. Wang, "FP-GNN: a versatile deep learning architecture for enhanced molecular property prediction," *Briefings in Bioinformatics*, vol. 23, no. 6, 2022.

[14] T. N. Kipf and M. Welling, "Semi-supervised classification with graph convolutional networks," 2016.

[15] O. Wieder, S. Kohlbacher, M. Kuenemann, A. Garon, P. Ducrot, T. Seidel, and T. Langer, "A compact review of molecular property prediction with graph neural networks," *Drug Discovery Today: Technologies*, vol. 37, pp. 1–12, 2020.

[16] D. Duvenaud, D. Maclaurin, J. Aguilera-Iparraguirre, R. Gómez-Bombarelli, T. Hirzel, A. Aspuru-Guzik, and R. P. Adams, "Convolutional networks on graphs for learning molecular fingerprints," 2015.

[17] J. Gilmer, S. S. Schoenholz, P. F. Riley, O. Vinyals, and G. E. Dahl, "Neural message passing for quantum chemistry," in *Proceedings of the 34th International Conference on Machine Learning*, ser. Proceedings of Machine Learning Research, D. Precup and Y. W. Teh, Eds., vol. 70. PMLR, 2017, pp. 1263–1272.

[18] K. Yang, K. Swanson, W. Jin, C. Coley, P. Eiden, H. Gao, A. Guzman-Perez, T. Hopper, B. Kelley, M. Mathea, A. Palmer, V. Settels, T. Jaakkola, K. Jensen, and R. Barzilay, "Analyzing learned molecular representations for property prediction," *Journal of Chemical Information and Modeling*, vol. 59, no. 8, pp. 3370–3388, 2019.

[19] J. Baek, M. Kang, and S. J. Hwang, "Accurate learning of graph representations with graph multiset pooling," 2021.

[20] R. Socher, D. Chen, C. D. Manning, and A. Y. Ng, "Reasoning with neural tensor networks for knowledge base completion," in *Advances in Neural Information Processing Systems*, C. Burges, L. Bottou, M. Welling, Z. Ghahramani, and K. Weinberger, Eds., vol. 26. Curran Associates, Inc., 2013, pp. 926–934.

[21] J. Degen, C. Wegscheid-Gerlach, A. Zaliani, and M. Rarey, "On the art of compiling and using 'drug-like' chemical fragment spaces," *ChemMedChem*, vol. 3, no. 10, pp. 1503–1507, 2008.

[22] P. Veličković, G. Cucurull, A. Casanova, A. Romero, P. Liò, and Y. Bengio, "Graph attention networks," 2017.

[23] K. He, X. Zhang, S. Ren, and J. Sun, "Identity mappings in deep residual networks," in *Computer Vision – ECCV 2016*. Springer International Publishing, 2016, pp. 630–645.

[24] D. Bahdanau, K. Cho, and Y. Bengio, "Neural machine translation by jointly learning to align and translate," 2014.

[25] Z. Wu, B. Ramsundar, E. N. Feinberg, J. Gomes, C. Geniesse, A. S. Pappu, K. Leswing, and V. Pande, "MoleculeNet: a benchmark for molecular machine learning," *Chemical Science*, vol. 9, no. 2, pp. 513–530, 2018.

[26] D. Fourches, E. Muratov, and A. Tropsha, "Trust, but verify: On the importance of chemical structure curation in cheminformatics and QSAR modeling research," *Journal of Chemical Information and Modeling*, vol. 50, no. 7, pp. 1189–1204, 2010.

[27] G. Landrum *et al.*, "RDKit: Open-source cheminformatics software (release 2022.03.2)," 2022.